



Femtosecond laser filaments for rapid and flexible writing of fiber Bragg grating

ERDEN ERTORER,* MOEZ HAQUE, JIANZHAO LI, AND PETER R. HERMAN

Institute for Optical Sciences, and the Department of Electrical and Computer Engineering, University of Toronto, 10 King's College Rd., Toronto, Ontario, M5S 3G4, Canada

*erdenertorer@gmail.com

Abstract: A new beam delivery method is introduced for controlling filament formation in optical fiber that enables point-by-point writing of 1st order fiber Bragg gratings (FBGs) with single femtosecond laser pulses. Uniform filament tracks with azimuthal symmetry were formed fully through the 9.3 μm core waveguide by a modified immersion focusing method to eliminate astigmatism by the cylindrical fiber shape. Filament arrays were precisely assembled inside of single-mode fiber, generating strong FBG resonances in the telecommunication band. Laser exposure control within this unique thin-grating geometry were key to manipulating the relative strength of the Bragg and cladding mode resonances while also independently tailoring their spectral resolution and features. This filament-by-filament writing rapidly forms gratings with highly flexible pattern control to tune wavelength, or introduce optical defects, demonstrated by a π -shifted FBG having a sharp 25 pm resonance embedded within a broader Bragg peak.

© 2018 Optical Society of America under the terms of the [OSA Open Access Publishing Agreement](#)

OCIS codes: (060.3735) Fiber Bragg gratings; (060.3510) Lasers, fiber; (320.7130) Ultrafast processes in condensed matter, including semiconductors; (140.3390) Laser materials processing.

References and links

1. K. O. Hill, Y. Fujii, D. C. Johnson, and B. S. Kawasaki, "Photosensitivity in optical fiber waveguides: Application to reflection filter fabrication," *Appl. Phys. Lett.* **32**(10), 647–649 (1978).
2. R. Kashyap, *Fiber Bragg Gratings* (Academic Press, 2009).
3. K. K. C. Lee, A. Mariampillai, M. Haque, B. A. Standish, V. X. D. Yang, and P. R. Herman, "Temperature-compensated fiber-optic 3D shape sensor based on femtosecond laser direct-written Bragg grating waveguides," *Opt. Express* **21**(20), 24076–24086 (2013).
4. J.-G. Liu, C. Schmidt-Hattenberger, and G. Borm, "Dynamic strain measurement with a fibre Bragg grating sensor system," *Measurement* **32**(2), 151–161 (2002).
5. A. Cusano, A. Cutolo, and J. Albert, *Fiber Bragg Grating Sensors: Recent Advancements, Industrial Applications and Market Exploitation* (Bentham Science Publishers, 2011).
6. D. Turchinovich, X. Liu, and J. Laegsgaard, "Monolithic all-PM femtosecond Yb-fiber laser stabilized with a narrow-band fiber Bragg grating and pulse-compressed in a hollow-core photonic crystal fiber," *Opt. Express* **16**(18), 14004–14014 (2008).
7. W. H. Glenn, G. Meltz, and E. Snitzer, "Method for impressing gratings within fiber optics," (1988).
8. G. Meltz, W. W. Morey, and W. H. Glenn, "Formation of Bragg gratings in optical fibers by a transverse holographic method," *Opt. Lett.* **14**(15), 823–825 (1989).
9. M. Becker, J. Bergmann, S. Brückner, M. Franke, E. Lindner, M. W. Rothhardt, and H. Bartelt, "Fiber Bragg grating inscription combining DUV sub-picosecond laser pulses and two-beam interferometry," *Opt. Express* **16**(23), 19169–19178 (2008).
10. A. Saliminia, A. Proulx, and R. Vallée, "Inscription of strong Bragg gratings in pure silica photonic crystal fibers using UV femtosecond laser pulses," *Opt. Commun.* **333**, 133–138 (2014).
11. A. Saliminia and R. Vallée, "Fiber Bragg grating inscription based on optical filamentation of UV femtosecond laser pulses," *Opt. Commun.* **324**, 245–251 (2014).
12. J. U. Thomas, C. Voigtländer, S. Nolte, A. Tünnermann, N. Jovanovic, G. D. Marshall, M. J. Withford, and M. Steel, "Mode selective fiber Bragg gratings," *Proc. SPIE* **7589**, 75890J (2010).
13. S. J. Mihailov, C. W. Smelser, P. Lu, R. B. Walker, D. Grobnic, H. Ding, G. Henderson, and J. Unruh, "Fiber bragg gratings made with a phase mask and 800-nm femtosecond radiation," *Opt. Lett.* **28**(12), 995–997 (2003).
14. A. Martinez, M. Dubov, I. Khrushchev, and I. Bennion, "Direct writing of fibre Bragg gratings by femtosecond laser," *Electron. Lett.* **40**(19), 1170–1172 (2004).
15. J. R. Grenier, L. a. Fernandes, P. V. S. Marques, J. S. Aitchison, and P. R. Herman, "Optical circuits in fiber cladding: Femtosecond laser-written Bragg Grating Waveguides," *Laser Sci. Photonic Appl.* **2**, 1–2 (2011).
16. K. Zhou, M. Dubov, C. Mou, L. Zhang, V. K. Mezentsev, and I. Bennion, "Line-by-line fiber bragg grating

- made by femtosecond laser,” *IEEE Photonics Technol. Lett.* **22**(16), 1190–1192 (2010).
17. P. Lu, S. J. Mihailov, H. Ding, D. Grobnic, R. Walker, D. Coulas, C. Hnatovsky, and A. Y. Naumov, “Plane-by-plane inscription of grating structures in optical fibers,” *J. Lightwave Technol.* **6**, 1 (2017).
 18. R. J. Williams, R. G. Krämer, S. Nolte, and M. J. Withford, “Femtosecond direct-writing of low-loss fiber Bragg gratings using a continuous core-scanning technique,” *Opt. Lett.* **38**(11), 1918–1920 (2013).
 19. C. Voigtländer, J. Thomas, E. Wikszak, P. Dannberg, S. Nolte, and A. Tünnermann, “Chirped fiber Bragg gratings written with ultrashort pulses and a tunable phase mask,” *Opt. Lett.* **34**(12), 1888–1890 (2009).
 20. B. Huang and X. Shu, “Line-by-Line inscription of phase-shifted fiber Bragg gratings with femtosecond laser,” in *Asia Commun. Photonics Conf.* (2015), paper ASu2A.60.
 21. S. Antipov, M. Ams, R. J. Williams, E. Magi, M. J. Withford, and A. Fuerbach, “Direct infrared femtosecond laser inscription of chirped fiber Bragg gratings,” *Opt. Express* **24**(1), 30–40 (2016).
 22. J. Burgmeier, C. Waltermann, G. Flachenecker, and W. Schade, “Point-by-point inscription of phase-shifted fiber Bragg gratings with electro-optic amplitude modulated femtosecond laser pulses,” *Opt. Lett.* **39**(3), 540–543 (2014).
 23. R. J. Williams, C. Voigtländer, G. D. Marshall, A. Tünnermann, S. Nolte, M. J. Steel, and M. J. Withford, “Point-by-point inscription of apodized fiber Bragg gratings,” *Opt. Lett.* **36**(15), 2988–2990 (2011).
 24. G. D. Marshall, R. J. Williams, N. Jovanovic, M. J. Steel, and M. J. Withford, “Point-by-point written fiber-Bragg gratings and their application in complex grating designs,” *Opt. Express* **18**(19), 19844–19859 (2010).
 25. Y. Li and T. G. Brown, “Radiation modes and tilted fiber gratings,” *J. Opt. Soc. Am. B* **23**(8), 1544–1555 (2006).
 26. C. Liao, J. He, Q. Wang, C. Zhang, Z. Li, C. Wang, and Y. Wang, “Fiber Bragg gratings Fabricated by Femtosecond Laser Micromachining Methods,” in *Opto-electronics and Communications Conference* (IEEE, 2015).
 27. G. H. Cheng, Y. J. Zhang, and Q. Liu, “Transmitting volume Bragg gratings in PTR glass written with femtosecond Bessel beams,” *Proc. SPIE* **10173**, 1017322 (2017).
 28. F. Ahmed and M. B. G. Jun, “Filament-Based Fabrication and Performance Analysis of Fiber Bragg Grating Sensors Using Ultrashort Pulse Laser,” *J. Micro Nano-Manufacturing* **2**(2), 21007 (2014).
 29. F. Ahmed and M. B. G. Jun, “Bragg grating fabrication in microfiber by femtosecond pulse filamentation induced periodic refractive index modification,” *Laser Appl. Microelectron. Optoelectron. Manuf.* **9350**, 93500C (2015).
 30. F. Ahmed and M. B. G. Jun, “Microfiber Bragg Grating Sandwiched between Standard Optical Fibers for Enhanced Temperature Sensing,” *IEEE Photonics Technol. Lett.* **28**(6), 685–688 (2016).
 31. Y. Lai, K. Zhou, K. Sugden, and I. Bennion, “Point-by-point inscription of first-order fiber Bragg grating for C-band applications,” *Opt. Express* **15**(26), 18318–18325 (2007).
 32. M. Haque, K. K. C. Lee, S. Ho, L. A. Fernandes, and P. R. Herman, “Chemical-assisted femtosecond laser writing of lab-in-fibers,” *Lab Chip* **14**(19), 3817–3829 (2014).
 33. J. R. Grenier, L. A. Fernandes, and P. R. Herman, “Femtosecond laser inscription of asymmetric directional couplers for in-fiber optical taps and fiber cladding photonics,” *Opt. Express* **23**(13), 16760–16771 (2015).
 34. J. R. Grenier, M. Haque, A. Fernandes, K. K. C. Lee, and R. Herman, “Femtosecond Laser Inscription of Photonic and Optofluidic Devices in Fiber Cladding,” in *Planar Waveguides and Other Confined Geometries* (2015).
 35. J. H. Marburger, “Self-focusing: theory,” *Prog. Quantum Electron.* **4**, 35–110 (1975).
 36. J. R. Grenier, L. A. Fernandes, and P. R. Herman, “Femtosecond laser writing of optical edge filters in fused silica optical waveguides,” *Opt. Express* **21**(4), 4493–4502 (2013).
 37. L. A. Fernandes, J. R. Grenier, P. R. Herman, J. S. Aitchison, and P. V. Marques, “Stress induced birefringence tuning in femtosecond laser fabricated waveguides in fused silica,” *Opt. Express* **20**(22), 24103–24114 (2012).
 38. T. Guo, F. Liu, B. O. Guan, and J. Albert, “Tilted fiber grating mechanical and biochemical sensors,” *Opt. Laser Technol.* **78**, 19–33 (2016).
 39. Y. Shevchenko, T. J. Francis, D. A. D. Blair, R. Walsh, M. C. DeRosa, and J. Albert, “In situ biosensing with a surface plasmon resonance fiber grating aptasensor,” *Anal. Chem.* **83**(18), 7027–7034 (2011).
 40. Z. Cai, F. Liu, T. Guo, B.-O. Guan, G.-D. Peng, and J. Albert, “Evanescently coupled optical fiber refractometer based a tilted fiber Bragg grating and a D-shaped fiber,” *Opt. Express* **23**(16), 20971–20976 (2015).

1. Introduction

Fiber Bragg gratings (FBGs) [1] find numerous applications in telecommunications [2], strain-based sensing for stress, temperature and shape monitoring [3–5], and fiber laser mirrors [6]. For weak intensity exposure, strong photosensitization responses are available with only ultraviolet lasers [7,8] and limited to narrow spectral regions that match with appropriate defect states. For this reason, the nonlinear optical interactions of femtosecond lasers are more flexible for embedding FBGs in more diverse types of optical materials found in today’s fibers [9–18].

Interference based exposure methods such as with phase-masks and beam splitters [9,10] are well developed for femtosecond processing, favoring the generation of uniform and long length gratings [11–13], but are inflexible in offering only limited wavelength tuning and spectral shaping of the FBG [9,19]. Hence, alternative methods such as point-by-point [14,15], line-by-line [16,20], plane-by-plane [17] and continuous core scanning [18,21] have emerged in direct writing of FBGs with femtosecond lasers, facilitating the formation of chirped [21], π -phase-shifted [22] and apodized [23] devices. These methods exploit various controls in shaping the focal volume of the focused femtosecond laser within the core waveguide, and extending the modification zone into the cladding, to enhance or diminish the degree of coupling to cladding and radiation modes [24,25]. Beam dithering [18] further improves the lateral uniformity of the grating elements to reach into the cladding zone and eliminate cladding and radiation mode coupling.

Since the overlapping of multiple exposures to create a single refractive index element is relatively slow for processing FBGs, single-pulsed femtosecond laser techniques have been developed to create a strong modification zone [18,24,26]. The geometry of the laser focus within the waveguide core volume is important here for manipulating the cladding and radiation mode coupling while retaining a strong FBG resonance. One can further exploit the geometry of elongated interaction zones by employing Bessel beams [27] or Kerr-lens self-focusing effects [28–30]. Ahmed et al. introduced femtosecond laser filamentation to fabricate FBGs by single-pulsed point-by-point exposure for strain sensing [28]. This approach yielded an excessively high bandwidth of 3.25 nm that may arise from filament distortions and break-up induced by the astigmatism of laser propagation through the cylindrical shaped fiber. Additional non-uniformity of the filament modification may arise from plasma generation effects at the high pulse energy (10 μ J) applied to the fiber, as well as due to beam propagation distortion in the proximity of pre-existing neighboring filaments.

In this paper, an improved method for filament formation is introduced for generating strong and high resolution FBGs in standard, single mode fiber. Astigmatism by the cylindrically shaped fiber was countered with a combination of glass plate and index matching oil in beam delivery [16,31] (Fig. 1), building on the oil-immersion focusing methods developed previously for fiber-cladding photonics and lab-in-fiber [32,33]. Single pulsed exposures were optimized for propagation through the plate and fiber to generate thin and uniform filament tracks with high aspect ratio, employing a combination of Kerr nonlinear and longitudinal aberration effects. The tracks could be assembled into tightly spaced arrays ($\Lambda = \sim 536$ nm) to reach the 1st order Bragg resonance for the ~ 1550 nm telecommunication band with only a weak birefringence. Exposure conditions are presented that provided a wide range of FBG coupling strength and spectral bandwidth, while also taking advantage of the thin-form factor of the grating to manipulate cladding mode spectral shape. A π -phase-shifted FBG is presented with an exceptionally narrow, 25 pm bandwidth, attesting to the precise alignment ($< \pm 1$ μ m) and assembly of the filament array within the 9.3 μ m core waveguide diameter.

2. Fabrication and characterization

The configuration for formation of self-focusing filament tracks into standard telecommunication fiber SMF-28 (Corning, NY, USA) is shown in Fig. 1. A Yb-doped fiber femtosecond laser (Satsuma, Amplitude Systemes) was frequency doubled to provide 515 nm wavelength and 250 fs pulse duration for strong interaction and tight focusing inside of the fused silica fiber material. Optimization of filament geometry was first evaluated in bulk fused silica glass with air and oil-immersion lens focusing. Optical microscopy showed that an aspherical air-focusing lens (NewFocus, 5722-A-H) of 0.55 NA to offer the most uniform, narrowest and highly contrasting filament tracks with lengths exceeding the 9.3 μ m diameter of fiber waveguide core. In order to avoid astigmatic focusing by the cylindrically shaped fiber, the beam delivery was modified to pass through a 1 mm thickness fused silica plate,

positioned parallel and in near-contact with the fiber. Refractive index matching oil (Fused Silica Matching Liquid, Code 50350, Cargille) filled the gap between the fiber cladding and the glass slide (Fig. 1), removing the cylindrical astigmatism of the fiber. However, a top-plate surface aberration is expected to stretch the depth of focus by $\sim 60 \mu\text{m}$ according to geometric optics, generating a beam profile with similar attributes of a non-diffracting Bessel beam [27]. Laser exposure was tested in the range of 316 nJ to 6 μJ per pulse to form weak to strong filament modification tracks without generating bubbles in the oil or damaging the cladding-air interface.

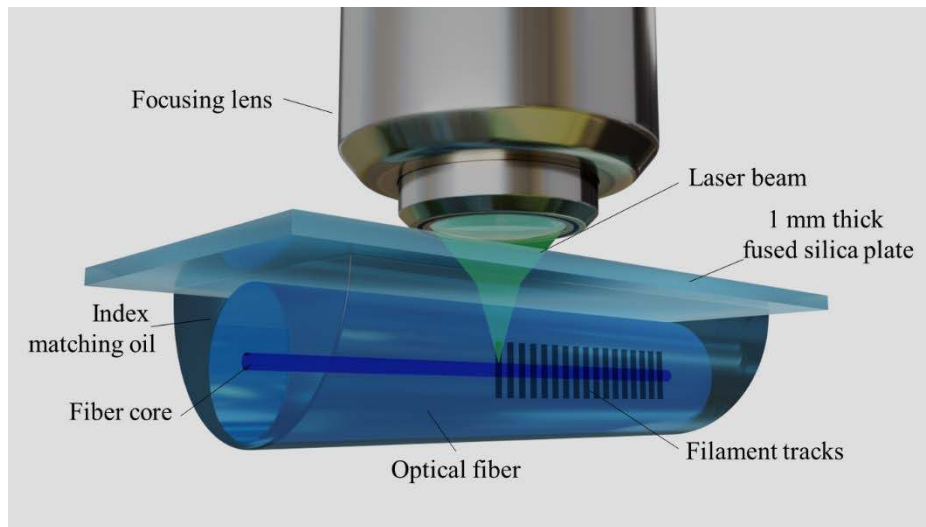


Fig. 1. Schematic of the oil-immersion focusing arrangement for eliminating astigmatic aberration during femtosecond laser writing of filament track Bragg gratings in the fiber core waveguide.

The filament track was evaluated with optical microscopy to ensure laterally centering to $\pm 1 \mu\text{m}$ precision relative to the core waveguide while generating filaments lengths that crossed the full core-waveguide cross-section. The laser repetition rate was down counted to the 1 Hz to 5 kHz range to improve the filament-to-filament positioning with reduced velocity and acceleration force on the fiber-plate assembly (Fig. 1). A grating period of $\sim 0.53 \mu\text{m}$ was selected with scanning speeds of 0.1 mm/s to 2mm/s, provided by a three-axis motion and alignment system (Aerotech-PlanarDL-200 XY and ANT130-060-L Z, Aerotech Inc.), thus generating 1st order FBG responses in the 1545 nm to 1555 nm wavelength range.

The assembly of linear-filament arrays was monitored in real time by launching broadband light (ASE-FL7002, Thorlabs) through the fiber during laser exposure and recording either transmission or reflection spectra with an optical spectrum analyser (AQ6317B, Ando). The birefringence properties of the FBGs were further characterized with free-space focusing optics and a linear polarizer aligned either parallel or perpendicular with the filament axis in the fiber.

FBGs were investigated for grating strength and bandwidth by varying the laser pulse exposure and the length of the grating. For the case of π -phase-shifted Bragg grating, a centrally positioned gap in the exposure zone was tuned to generate a strong, narrow and centrally positioned optical defect in the FBG spectrum.

3. Results

In the case of direct air focusing into the fiber, aspherical air lenses were unable to create long and uniform filament tracks that fully extended through the fiber core due to the cylindrical aberration of the fiber shape. Such aberration was avoided with a 1.25 NA oil immersion lens

[32,34], but the high NA restricted the filament length while also producing micro-explosion voids, a Type III modification that distorted the ideal filament shape of refractive index structure. The pulse energy required for generating filament tracks was also significantly higher than previously used for writing waveguide or nanograting tracks [32,34], and exceeded the threshold for burning and generating air bubbles in the immersion oil, thus causing beam distortion effects. Study of filament formation with air focusing in bulk fused silica pointed to an optimal 0.55 NA lens when focusing deeply (i.e. ~ 1 mm), providing highly contrasting, high aspect ratio and uniform filament tracks of ~ 60 μm length. This process was transferred to the fiber by using the same lens in combination with a 1 mm thick fused silica glass plate, made to contact the fiber as shown in Fig. 1. This arrangement minimized the volume of refractive index matching oil that would be susceptible to burning and bubble generation. In this way, uniform filament modifications with azimuthal symmetry were created across the full cross-section of the core waveguide.

The morphology and positional control of laser filament formation inside the optical fiber are presented in the optical microscope images of Fig. 2 for exposure conditions in a range of 316 nJ to 6 μJ energy per pulse. Figure 2(a) shows isolated filament modification tracks were formed with controllable length, contrast and uniformity. At the visual detection limit of 1.5 μJ pulse energy (left), the ~ 1 μm wide modification track extends up to ~ 60 μm length, offering a high aspect ratio of greater than 60. These tracks extend more than 40 times longer than the 1.4 μm depth of focus of the 0.55 NA lens. The tracks are unbroken, and consist of a dark central zone of negative refractive index change which transitions to a positive change (white zones) both above and below the stronger central interaction zone. For increasing pulse energy from 1.5 μJ to 6 μJ (left to right in Fig. 2(a)), the filament tracks grow longer, but become less uniform and more discontinuous, dividing more sharply between a larger zone of stronger negative refractive index change sandwiched by the positive index zones. Kerr self-focusing effects are evident in the movement of the filament track position upward as expected towards the laser source in Fig. 2(a) with the increasing pulse energy. All these exposures exceed the threshold pulse energy of 200 nJ, calculated for self-channeling [35]. However, the contribution of self-channeling in the filament track formation could not be separated from the effect of focal blurring and elongation (i.e. ~ 60 μm) arising due to the top-surface aberration effect.

The energy-dependent filament positioning was compensated by translation of the fiber alignment stages vertically, for example, with the 5 μm offsets as shown in Fig. 2(b) for a fixed 3 μJ pulse energy. In this way, filament tracks could be centered vertically in the core waveguide for each laser exposure energy. Filament tracks were assembled into a dense grating array of ~ 0.53 μm period, as required for telecommunication band FBGs, by centering the most uniform part of the negative index zone in the core waveguide. The resulting grating is shown unresolved in Fig. 2(c) due to the microscope resolution. The filament array is visually observable for this ~ 1.0 μJ pulse energy, but the refractive index contrast appears washed out relative to the isolated filament cases (Fig. 2(a)), possibly owing to relaxation or erasure mechanisms of the photosensitivity response when the filament zones are closely overlapping. At lower pulse exposure of 360 nJ, the filament arrays are no longer observable by an optical microscope but appear lit up as shown in the side (Fig. 2(d)) and end (Fig. 2(e)) grating views when red light was coupled into the fiber core waveguide. Strong radiation modes are expected in this fiber with the combination of thin linear grating geometry, 635 nm probe wavelength and 0.53 μm grating period. The optical radiation was emitted only from the filament array, narrowing in Fig. 2(d) to the ~ 1 μm grating thickness from inside of the 9.3 μm core-waveguide diameter. The thin grating features are also evident in the end facet view of the same illuminated grating, when cleaved through the grating zone as shown in Fig. 2(f). Figures 2(d) and 2(f) confirm the filament grating formation has reached through the full diameter of core waveguide with a high ± 1 μm centering accuracy with respect to the central fiber axis.

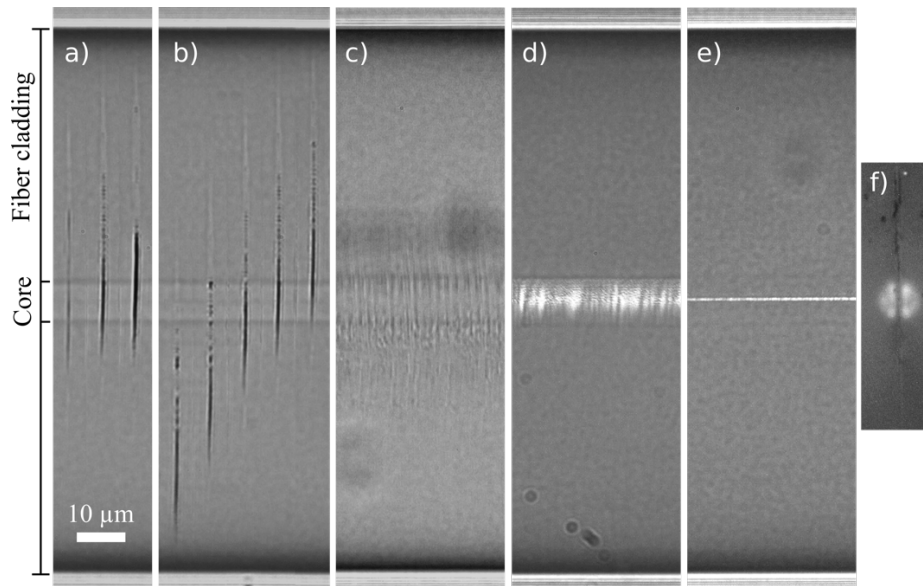


Fig. 2. Optical microscope images of isolated filamentation tracks (a-b) and Bragg grating arrays of $0.536 \mu\text{m}$ spacing (c-f), aligned inside the core waveguide of fiber, formed with a) 1.5, 3 and 6 μJ pulse energy (left to right) at same focal depth position, b) 3 μJ pulse energy at various focal depths, (c) 1 μJ pulse energy, and 360 nJ pulse energy, where scattering of red waveguiding light confirms formation of a narrow grating structure fully through the core waveguide in d) side view, e) top view, and f) end facet view.

The strongly contrasting morphology of the filament gratings that are apparent in Figs. 2(a)-2(c) were found to generate strong and broad Bragg grating resonances, but with a high insertion loss when the laser exposure exceeded $1 \mu\text{J}/\text{pulse}$. Transmission spectra of FBGs are shown in Fig. 3(a) for a moderate exposure of 480 nJ/pulse, demonstrating fast growth of the Bragg resonance dip from 4.8 dB to 28 dB with increasing grating length from only 1 mm to 4 mm. The spectra were similar whether the cladding was surrounded by air or immersed in index matching fluid. A strong AC modulation refractive index is thus confirmed for the 1st order FBGs. The Bragg resonance is broad, at 604 pm, while also generating a strong scattering loss of 0.80 dB/cm at long wavelength ($>1546 \text{ nm}$). The asymmetry of the $\sim 1 \mu\text{m}$ thin grating geometry against the $10.4 \mu\text{m}$ mode field diameter underpins the strong coupling to cladding modes seen in the 2 dB to 10 dB deep loss bands that are broaden and reach from 1541 nm to 1544 nm wavelength as shown partially in Fig. 3(a). This cladding mode spectrum begins as a continuum for short grating length, and develops discrete resonances with increasing length. The Bragg resonance and cladding mode coupling could be favorably manipulated by the relative grating position in the core waveguide as well as by the laser pulse energy.

The growth of the Bragg resonance strength in Fig. 3(a) was found to closely follow standard models for uniform gratings according to:

$$R = \tan h^2(K_{AC}L_g). \quad (1)$$

where K_{AC} is the AC coupling coefficient and L_g is the grating length. The reflectivity, R , of the Bragg resonance was inferred from the observed transmission dip, T_{dip} , according to $R = 1 - 10^{-\frac{T_{\text{dip}}(\text{dB})}{10}}$, and plotted as function of grating length in the inset image (Fig. 3(a)). A best fit of the reflectivity data (solid line) by Eq. (1) yielded a strong coupling value of $K_{AC} = 1.67 \text{ mm}^{-1}$ with a low fitting error (RMSE = 0.0236) for this 480 nJ pulse energy exposure and 1 mm to 4 mm length.

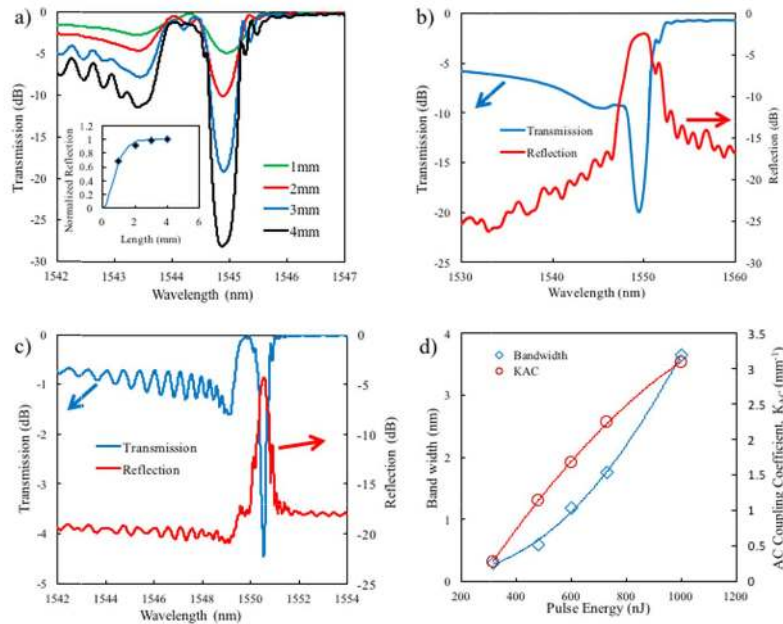


Fig. 3. Spectral responses of FBGs formed in single mode optical fiber with femtosecond laser self-focusing filaments: a) transmission spectra for increasing grating length at 480 nJ pulse energy, and inset shows the change in the reflectivity as a function of grating length; and transmission and reflection spectra for b) a strong 1.6 mm long FBG by 1 μ J pulse energy and c) a weak 5 mm long FBG by 316 nJ pulse energy. d) Pulse energy dependency of AC coupling coefficient K_{AC} and 3dB bandwidth of Bragg resonance.

Figure 3(b) shows the effect of higher exposure where a broad 2.48 nm wide resonance with 20 dB transmission dip was reached in only 1.6 mm length and with 1 μ J/pulse energy. The propagation loss increased to 4.37 dB/cm due to stronger radiation modes, which reduced the on-resonant Bragg reflection by 2.4 dB. Cladding mode coupling appears as a broad continuum that exceeds 5 dB loss and is approaching an edge filter device as previously reported in [36] with high NA point-by-point FBG writing.

In the limit of weakest laser exposure of 316 nJ/pulse, moderate-strength Bragg resonances of 4.5 dB and 5.0 dB are seen in transmission and reflection spectra, respectively, to form with a narrow bandwidth of 300 pm (full width at -3 dB), as shown in Fig. 3(c) for a 5 mm long grating. Cladding mode coupling has weakened and also narrowed into isolated modes of ~ 1.6 dB peak transmission loss. The more gentle laser modification has favorably reduced the propagation loss to 0.013 dB/cm. FBG resonances could not be observed for lower exposure of 290 nJ for gratings up to 2 cm length, which is consistent with a sharp onset threshold energy inferred at ~ 300 nJ by extrapolation of the K_{AC} data in Fig. 3(d).

The FBG spectral features are seen to have a strong dependency on the pulse energy used to form the filaments. The overall trend of increasing Bragg grating strength and bandwidth with an increase in laser pulse energy is presented in Fig. 3(d) over the 316 nJ to 1 μ J/pulse range found to generate low to moderate loss gratings. The observations reveal strong Bragg resonances in both transmission and reflection spectra, readily exceeding 20 dB in transmission for grating lengths of less than 5 mm length. These results underscore a strong refractive index modulation, with the coupling coefficient reaching as high as $K_{AC} = 3.1 \text{ mm}^{-1}$ in Fig. 3(c). The Bragg resonances strengthened systematically with increasing laser exposure and length, closely following the traditional response as in Eq. (1). However, the filament grating was seen (e.g. Figure 3(a)) to begin formation from a wide Bragg resonance, except when writing with near-threshold exposure of ~ 316 nJ/pulse when 300 pm bandwidth was

observed. Similarly, the grating structures induce large propagation losses, rising from 0.8 dB/cm at a moderate 480 nJ exposure. Lower exposure of ~ 316 nJ/pulse is therefore desirable to reduce loss to 0.013 dB/cm. The minimum exposure for observing refractive index contrast, shown at 360 nJ/pulse exposure in Fig. 2(c), may thus represent low-damage modification, but transitioning to Type II damage response as higher exposure generates stronger Bragg coupling and line broadening (Fig. 3(b)). The FBG spectral features transition towards an edge-filter response [36] at $1.5 \mu\text{J/pulse}$ as the contrast in refractive index sharpens as shown Fig. 2(a) from $1.5 \mu\text{J}$ to $3 \mu\text{J}$ pulse energy. The novel thin grating geometry (Figs. 2(d) to 2(f)) offers unique advantages for exciting strong cladding modes and manipulating the discrete to broad resonance spectral structures as presented in Fig. 3. The filament grating has provided these advantages with the same Bragg grating features and strength as demonstrated with other femtosecond laser methods, based on single or multi pulsed writing in point-by-point and line-by-line focusing.

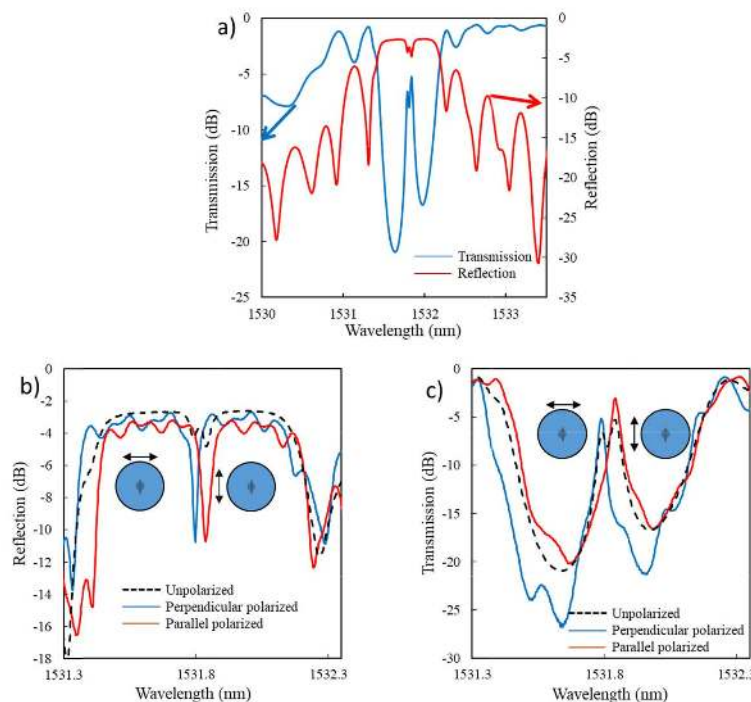


Fig. 4. Transmission (a,c) and reflection (a,b) spectra of a π -phase-shifted FBG formed over 4 mm length with 360 nJ/pulse energy, probed with unpolarized light (a) and with linear polarized light (b,c) aligned parallel and perpendicular with the filament grating.

In order to examine the flexibility of filament-by-filament writing of FBGs, π -shifted gratings were generated to improve on the grating resolution and test for waveguide birefringence. Figure 4(a) shows transmission and reflection spectra for a moderately weak exposure of 360 nJ/pulse and 4 mm grating length, where the π -shift was physically centered in the grating. The two narrow transmission dips of 26 pm appear centered in each of the stop bands. The peak-to-peak offset of $\Delta\lambda = 50$ pm indicates a birefringence that is much smaller than the overall 0.77 nm FBG bandwidth.

By launching linearly polarized light aligned either parallel or perpendicular with respect to the filament orientation, isolated π -shift defects were uncovered for each polarization as

shown in the reflection and transmission spectra of Figs. 4(b) and 4(c), respectively. In reflection, the isolated polarization states reveal a moderately strong π -shifted resonance of ~ 10 dB depth while the transmission resonance shows a high resolution peak of ~ 25 pm at 3 dB full width. The peak-to-peak polarization offset of 50 pm here corresponds to a weak but nonzero birefringence of 4.67×10^{-5} for the 360 nJ/pulse grating.

4. Discussion

The elongated interaction zone of self-focused femtosecond laser pulses permitted a high-resolution line-by-line writing of thin volume gratings precisely centered in the core waveguide of single-mode fiber. A 316 nJ to 1 μ J processing window for single pulse writing was identified for creating strong and highly contrasting refractive index structures that supported 1st order Bragg resonances ($\Lambda = \sim 0.53$ μ m period) in short grating length < 5 mm. The gratings offered relatively low loss (~ 0.013 dB/cm) and narrow linewidth (300 pm) with exposures tuned near the threshold for grating formation. The precision of the filament-by-filament writing was demonstrated in the formation of a sharp π -phase-shift grating in Fig. 4. A weak $\Delta n = 4.67 \times 10^{-5}$ birefringence may be inherent in the asymmetry of a strong refractive index contrast formed in the shape of a single-pulse filament that contrasts with the more symmetric focusing geometries employed in other laser writing approaches. Such waveguide birefringence may be tuned or eliminated by employing femtosecond laser stressing tracks as in [37]. The demonstration of π -phase-shifted FBG confirms that highly organized and coherent structuring is possible by filament arrays over short or long fiber lengths. The 25 pm bandwidth of π -shifted FBG is promising for high-resolution laser mirror and sensing applications.

The novel thin-plane geometry of filament gratings offers flexible options for controlling cladding mode coupling and manipulating the shape of transmission spectra (Figs. 2(a) and 2(c)). While such cladding mode loss is undesirable for telecommunication applications, selective excitation of cladding mode light has been harnessed for various forms of sensing such as with evanescent or plasmonic devices [38–40]. These benefits can be preferentially obtained in short devices with modest laser exposures up to ~ 1 μ J/pulse before being limited by losses exceeding 1 dB/cm.

Reaching a narrow FBG bandwidth requires formation of highly uniform filament tracks, depending fundamentally on a balancing between the Kerr lensing effect and plasma defocusing. Further study of the focusing geometry with variation in laser pulse duration, beam shape and laser wavelength are promising directions to improve on the present filament writing methods for FBG writing, and manipulate cladding and radiation modes, as well as the strength, birefringence, and shape of the Bragg resonance. Lastly, improvements in beam delivery may permit one to fully harness high MHz repetition rates, permitting grating writing speeds to accelerate from seconds here to sub-milliseconds.

5. Conclusion

A new, damage-free beam delivery method has been introduced to overcome astigmatic focusing of femtosecond laser pulses and generate uniform, azimuthally symmetric filaments in optical fiber. The point-by-point writing enabled 1st order Bragg gratings to form rapidly in the telecommunication band with high strength and in short lengths. The unique planar geometry affords benefits in manipulating the coupling to cladding and radiation modes. The relative strength and bandwidth features of the Bragg resonance and cladding mode loss could be selectively tuned with the laser pulse energy. The flexibility of such filament-by-filament direct writing was exemplified by formation of a π -phase-shifted FBGs with a narrow 25 pm single-polarization resonance.

Funding

NSERC Strategic Partnerships Project 447284.